TU Delft

Delft University of Technology

Design and testing of a low subsonic wind tunnel gust generator

Lancelot, Paul M.G.J.; Sodja, Jurij; Werter, Noud P.M.; De Breuker, Roeland

DOI
10.12989/aas.2017.4.2.125

Publication date
2017

Document Version
Accepted author manuscript

Published in
Advances in Aircraft and Spacecraft Science

Citation (APA)
Lancelot, P. M. G. J., Sodja, J., Werter, N. P. M., & De Breuker, R. (2017). Design and testing of a low subsonic wind tunnel gust generator. *Advances in Aircraft and Spacecraft Science*, *4*(2), 125-144. https://doi.org/10.12989/aas.2017.4.2.125

Important note
To cite this publication, please use the final published version (if applicable).
Please check the document version above.

Copyright
Other than for strictly personal use, it is not permitted to download, forward or distribute the text or part of it, without the consent of the author(s) and/or copyright holder(s), unless the work is under an open content license such as Creative Commons.

Takedown policy
Please contact us and provide details if you believe this document breaches copyrights.
We will remove access to the work immediately and investigate your claim.

This work is downloaded from Delft University of Technology.
For technical reasons the number of authors shown on this cover page is limited to a maximum of 10.

Design and testing of a low subsonic wind tunnel gust generator

Paul M.G.J. Lancelot*, Jurij Sodja, Noud P.M. Werter, and Roeland De Breuker

Delft University of Technology
Kluyverweg 1, 2629 HS Delft, The Netherlands

Abstract. This paper summarises the design of a gust generator and the comparison between high fidelity numerical results and experimental results. The gust generator has been designed for a low subsonic wind tunnel in order to perform gust response experiments on wings and assess load alleviation. Special attention has been given to the different design parameters that influence the shape of the gust velocity profile by means of CFD simulations. Design parameters include frequency of actuation, flow speed, maximum deflection, chord length and gust vane spacing. The numerical results are compared to experimental results obtained using a hot-wire anemometer and flow visualisation by means of a tuft and smoke. The first assessment of the performance of the gust generator showed proper operation of the gust generator across the entire range of interest.

Keywords. Gust generator, computational fluid dynamics, fluid structure interaction, experimental aerodynamics, experimental aeroelasticity

---

1. Introduction

Gust encounter is among the most critical load cases an aircraft can experience during service life. The increasing aspect ratio of modern commercial aircraft wings and reducing weight generally result in an increased sensitivity of the wing to gust loads. Researchers have been looking for solutions to reduce structural stresses at the wing root caused by gust encounters, either by using passive (e.g. aeroelastic composite tailoring) or active methods (e.g. deploying control surfaces). Reducing loads reduces airframe weight and hence operational cost of the aircraft. In order to ease the development of these methods, many computational techniques of different fidelity levels have been developed to evaluate the structural response to gust loads. Nonetheless, the unsteady nature of a gust flow and strong coupling between resulting aerodynamic loads and structural deformations make the modelling of a pertinent dynamic response a challenging task. Hence code validation is necessary. In order to perform such experiments in a wind tunnel a gust generator is required. Hence, many research institutes and universities have been building such systems for the purpose of their own research. Table 1 is a summary of the different gust

* Corresponding author, Ph.D. Student, E-mail: p.m.g.j.lancelot@tudelft.nl

generators that have been in operation during the past 50 years. Gust generator development is driven primarily (a) by experiment requirements and (b) by the available wind tunnel facilities.

Table 1 Summary of existing gust generator installations around the world. If the top speed achieved during gust experiments isn't available, the maximum speed of the wind tunnel is written instead.

Research Institute/University	**Year**	**Top speed**	**Wind tunnel cross section**
NASA (USA) (Reed, 1981)	1966	Mach 1.2	Square 4.9 × 4.9 m^2
MIT (USA) (Ham et al., 1974)	1974	37 m/s	Elliptical 2.13 × 3.32 m^2
Duke University (USA) (Tang et al., 1996)	1996	25 m/s	Rectangular 0.7 × 0.53 m^2
Virginia Tech (USA) (Grissom and Devenport, 2004)	2004	15 m/s	Square 2.15 × 2.15 m^2
TSAGI (Russia) (Kuzmina et al., 2005)	2005	30 m/s	Elliptical 4.0 ×2.33 m^2
TSAGI (Russia) (Kuzmina et al., 2005)	2005	120 m/s	Circular 7 m diameter
University of Maryland (USA) (Koushik and Schmitz, 2007)	2008	N/A	N/A
Politecnico di Milano (Italy) (Ricci and Scotti, 2008)	2008	30 m/s	Rectangular 1.0 × 1.5 m^2
University of Colorado,(USA) (Roadman and Mohseni, 2009)	2009	20 m/s	Square 0.34 × 0.34 m^2
DLR (Germany) (Neumann and Mai, 2013)	2010	Mach 0.75	Square 1.0 × 1.0 m^2
ONERA (France) (Lepage et al., 2015)	2011	Mach 0.73	Rectangular 0.76 × 0.8 m^2
Beihang University (China) (Wu et al., 2013)	2012	24 m/s	Square 3 × 3 m^2
Cal Poly Pomona (USA) (YouTube video)	2013	61 m / s	Rectangular 1.0 × 0.71 m^2
Cranfield University (England) (Saddington et al., 2014)	2015	14.5 m/s	Elliptical 1.52 ×1.14 m^2
ARA (England) (Allen and Quinn, 2015)	2015	Mach 0.85	Rectangular 2.74 × 2.44 m^2
Politecnico di Milano (Italy) (S.Ricci et al, 2015)	2016	55 m/s	Rectangular 4.0 × 3.84 m^2
Mitsui engineering (Japan) (San technologies website)	N/A	20 m/s	N/A
JAXA (Japan) (Kenichi et al. 2015)	N/A	Transonic	N/A

Different ways of producing a gust have been explored. Most gust generators use one or multiple oscillating aerofoils in pitch to produce the required gusts, however alternatives solutions exist. The design proposed by Tang et al., (1996) uses a rotating slotted cylinder, which has the advantage that it requires very low torque and power input. On the other hand, the maximum gust angle that can be achieved with this method is lower compared to what is possible with pitching aerofoils. Roadman and Mohseni (2009) used an active grid to generate continuous turbulence with little actuation power. This solution, however, cannot produce a "1-cos" gust as prescribed by the certification (EASA, 2012). The recently built gust generator at the Aircraft Research Association (ARA) (Allen and Quinn, 2015) uses blowing air jets mounted on two fixed profiles to generate the gust flow, which was required because it is designed to operate under transonic flow conditions, within a large wind tunnel section. Finally the NASA gust generator for the Transonic Dynamic Tunnel (Reed, 1981) which also operates in the transonic regime generates a gust with small pitching surfaces mounted on the side wall of the tunnel. These pitching surfaces don't span the entire width of the wind tunnel's section.

Most applications of a gust generator are related to aircraft wing design and experiments. Gust response experiments on flexible wings have been carried out, either on a clamped wing (Neumann and Mai, 2013) or on a wing mounted on a free flying aircraft model (Reed, 1981). Furthermore, active gust load control has been investigated, for a clamped wing (Ricci and Scotti, n.d.), for an aircraft half model (Wu et al., 2013), and with a two degree of freedom aeroelastic apparatus (Lepage et al., 2015). One experiment conducted at TSAGI using the European Research Aeroelastic Model (EuRAM) (Kuzmina et al., 2005) featured a combination of passive and active gust load alleviation devices. Finally, some experiments were also dedicated to micro aerial vehicles (MAV) (Roadman and Mohseni, 2009; Saddington et al., 2014) and helicopter blades (Koushik and Schmitz, 2007).

The wind tunnel used at the Delft University of Technology is the Open Jet Facility (OJF), featuring a test section of 2.85 × 2.85 m^2 and with a flow speed of up to 35m/s. The goal of the gust generator is to produce a discrete gust to evaluate load alleviation and the gust response of tailored composite wings, as illustrated in Fig. 1. As the OJF is a multi-purpose wind tunnel, the gust generator should also be suitable for gust response experiments of wind turbines and MAVs.

This paper presents the design of the gust generator. Initial studies and trade-offs between different design parameters are first presented, followed by the experimental setup description and the results of the preliminary tests with sine wave gusts.

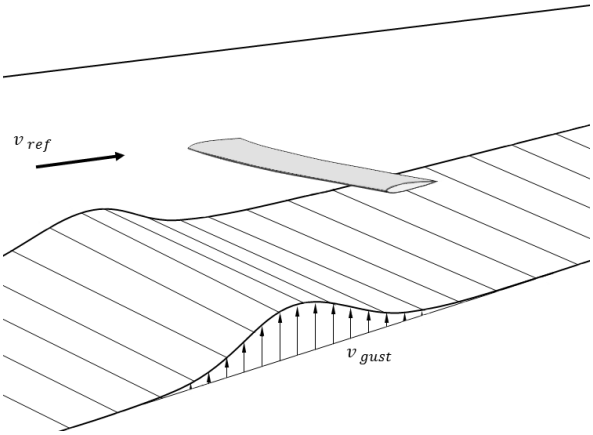

Fig. 1 Illustration of a wind tunnel load alleviation experiment using a cantilevered wing and a discrete gust. v_{ref} represents the free stream flow speed and v_{gust} the gust speed.

2. Preliminary design study

Gust generator requirements are discussed first. Then the application of CFD simulations used to identify the key design parameters and to optimise the gust generator performance is explained. Next, the wind tunnel and the overall experimental setup are presented followed by the discussion of the fluid-structure interactions (FSI) simulations used to investigate the structural behaviour of the gust generator. Finally, the actuation system used to move the gust vanes is presented as well.

2.1 Requirements

The gust generator target performance is based on the CS23 certification from the European Aviation Safety Agency (EASA, 2012). Accordingly, the evolution of the amplitude of a discrete gust is defined as follows:

$$v_{gust} = \frac{v_G}{2}\left(1 - \cos\frac{2\pi s}{25\bar{C}}\right) \tag{1}$$

where v_G denotes the maximum gust amplitude, *s* the distance traveled by the aircraft inside the gust, and $\bar{C}$ its mean aerodynamic chord. The gust frequency, *f*, that needs to be attained inside the wind tunnel can be determined from *s* as:

$$s = v_{ref} \cdot t \tag{2}$$

$$f = \frac{v_{ref}}{25\bar{C}} \tag{3}$$

The maximum speed allowed in the wind tunnel for this type of experiment is 25 m/s, and, thus, v_{ref} is equal to 25 m/s. Besides the flow speed, the frequency is also a function of the mean aerodynamic chord, $\bar{C}$, of the aircraft that encounters the gust. The expected wings to be tested will have a chord length varying from 0.2 m to 0.4 m. From Eq. (3) it follows, that the gust frequencies should range from 5 Hz to 2.5 Hz respectively. Therefore, to comply with the gust requirements from the EASA certification, the gust generator needs to be able to produce a gust with a frequency of 5 Hz at a flow speed of 25 m/s.

Most of the results in this paper are formulated with respect to the gust angle, to be able to compare the change in angle of attack induced by the gust at different flow speeds:

$$\alpha_{gust} = \tan^{-1}\left(\frac{v_{gust}}{v_{ref}}\right) \tag{4}$$

2.2 Preliminary study of the gust generator

The gusts are produced by two rectangular gust vanes with a symmetric airfoil oscillating in pitch around an axis located at 23.7% chord. Comparisons between flow measurements and simulations from Dequand et al., (2011), Grissom and Devenport, (2004) and Neumann and Mai, (2013) have shown that having two gust vanes is a good compromise between gust quality and setup complexity.

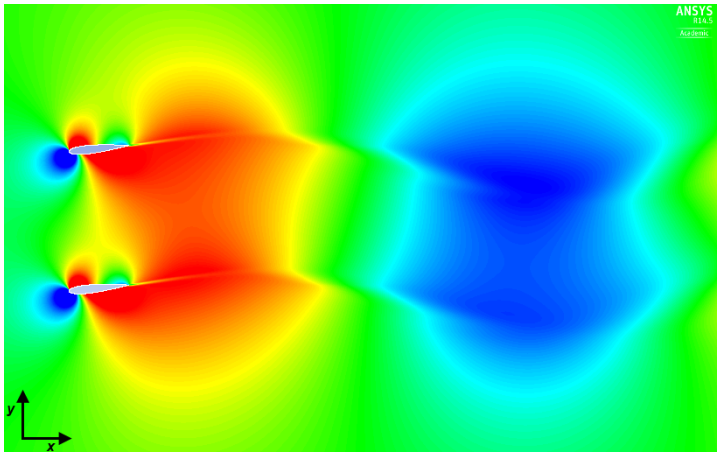

Fig. 2 Contours of the gust angle for a time transient CFD simulation with ANSYS Fluent.

The gust uniformity is critical to investigate the intended gust response of the wing. In the experiment by *DLR* (Neumann and Mai, 2013), having only one gust vane penalises the uniformity of the gust in space, since an important shear flow region due to the airfoil boundary layer is created in the wake behind the gust generator. Adding a second gust vane, and placing the test wing in-between both vanes avoids this effect. The shear flow region can be seen in Fig. 2. Increasing the number of gust vanes is an option to further increase gust uniformity if necessary, however it might result in an unwanted interaction between the model and the gust generator's shear flow area in the wake if the vanes need to be placed too close together.

2D transient flow simulations have been done to evaluate how the gust flow reacts to different types of gust vane motion and geometry. ANSYS Fluent is used, with an incompressible flow solver and the Spalart-Allmaras turbulence model. A convergence study was carried out, resulting in a time step of 0.002 seconds and a mesh of 100.000 deformable rectangular elements, as shown in Fig. 3 and Fig. 4. For the sake of simplicity, the full interior of the Open Jet Facility is not modelled. The motion of the vanes is directly simulated by pitching the airfoils, around the quarter-chord point using FLUENT's user defined functions (UDFs).

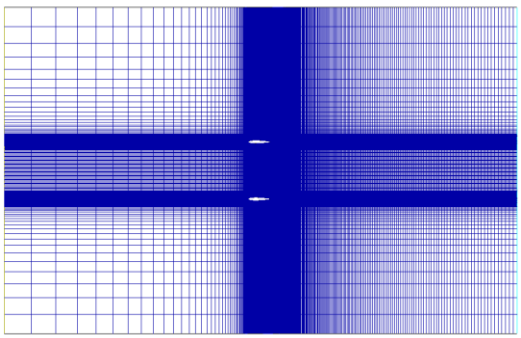
Fig. 3 Structured 2d CFD grid.

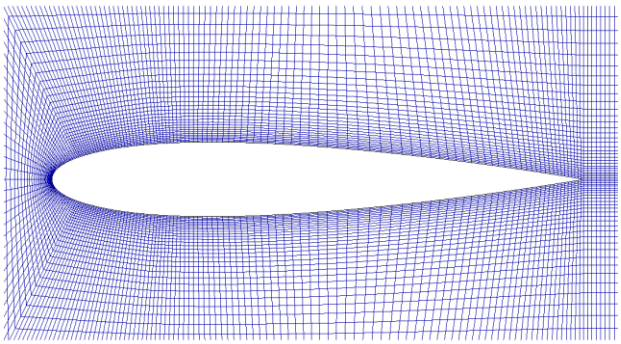
Fig. 4 Close up on one of the gust vanes.

Design variables important to gust generator performance and sizing are summarised in Table 2.

Table 2 Design variables

Design variables	Values evaluated
Chord length of the gust vanes: c	0.2 m, 0.3 m, 0.4 m
Space between the gust vanes: dh	0.3 m, 0.5 m, 0.7 m
Reduced frequency: $k = \pi f c / v_{ref}$	0.0377, 0.113, 0.1884
Maximum angle of deflection of the gust vanes: δ_{max}	2.5, 5, 10 degrees

Note that, during a gust response experiment, the vane chord length, c, is the only parameter which cannot be adjusted, while, the spacing, dh, reduced frequency, k, and maximum angle of deflection can be adjusted within the bounds of the gust generator capabilities.

First the effect of the gust vane chord length was investigated. Fig. 5 shows the resulting gust angles obtained at constant flow velocity and frequency of actuation. A linear relation between the maximum gust angle, α_G, and the gust vane chord length is observed.

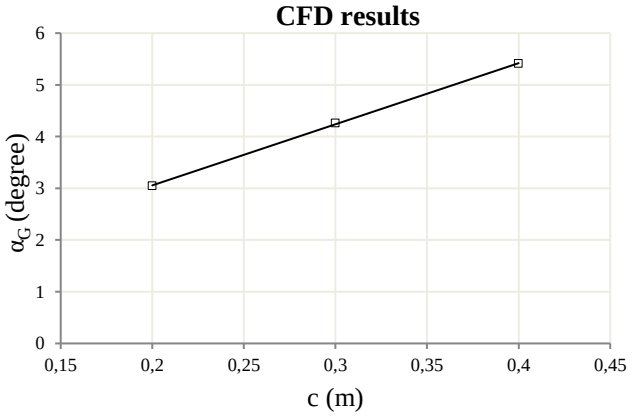

Fig. 5 The maximum gust angle computed for different chord lengths. These measurements are taken 1.5 m behind the leading edge of the gust vanes, in the center axis of the fluid domain. $\delta_{max} = \pm 10$ degrees.

The next parameter under investigation is the spacing between the gust vanes. The flow interaction between two gust vanes has already been studied numerically by *Dequand et al.* (2011) who concluded that some interaction can occur, if the two vanes are too close to each other, which alters the shape of the gust.

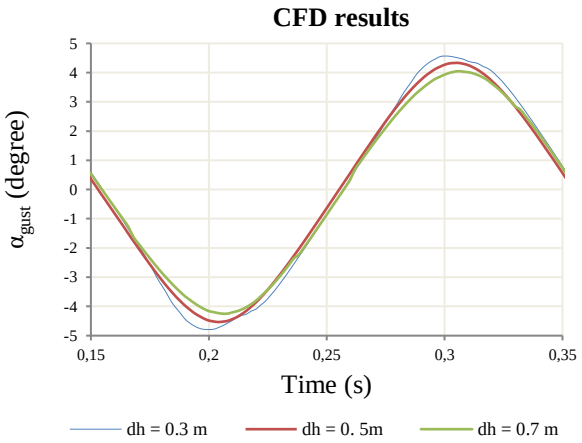

Fig. 6 Variation of gust angle with time for different vane spacing. c = 0.3 m, v_{ref} = 25 m/s, f = 5 Hz and δ_{max} = ±10 degrees.

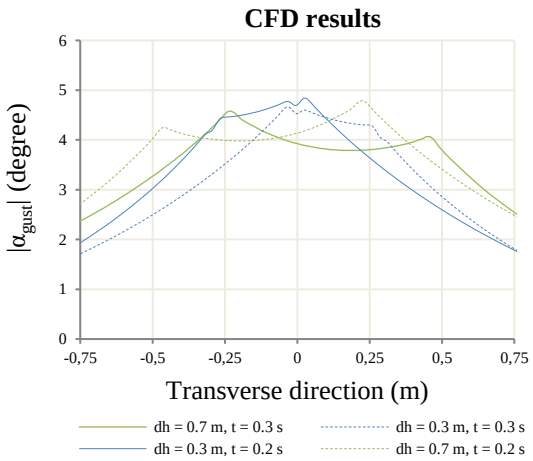

Fig. 7 Gust amplitude variation in the transverse direction for different vane spacing. c = 0.3 m, v_{ref} = 25 m/s, f = 5 Hz and δ_{max} = ±10 degrees.

Similar observations can be made in Fig. 6, showing a change in the shape of the gust profile as the vanes get closer. Fig. 7 shows the variation of the gust velocity profile in the transverse direction at two different times for dh = 0.7 m and dh = 0.3 m. Due to the interaction between the two vanes one can observe different lateral gust profiles at different phase angles in the gust vane oscillation cycle. This effect is more pronounced at dh = 0.3m, where the test model located behind the gust generator will always be subjected to the shear flow region. Hence, having a larger spacing between the two gust vanes is better for the quality of the experiment. The flow interactions can also be seen in Fig. 2.

The effect of reduced frequency variation is investigated next. Reduced frequency, *k*, is defined as:

$$k = \frac{\pi f c}{v_{ref}} \tag{5}$$

where f is the frequency in Hz, and c is the chord length of the vanes. In the following results, a constant chord length of 0.3 m has been chosen and the reduced frequency is varied by means of the gust frequency and flow speed. Therefore a test matrix shown in Table 3 has been defined, which was followed during both numerical and experimental investigations.

Table 3 Operational actuation frequency and flow speed

Reduced frequency *k*	**Wind tunnel reference speed v_{ref}**		
	15 m/s	21 m/s	25 m/s
0.0377	*f = 0.6* Hz	*f = 0.84* Hz	*f = 1* Hz
0.1130	*f = 1.8* Hz	*f = 2.52* Hz	*f = 3* Hz
0.1884	*f = 3* Hz	*f = 4.2* Hz	*f = 5* Hz

In Fig. 8, it can clearly be seen that the same reduced frequency at different flow speeds results in the same gust amplitude. Furthermore, it can be seen that the gust angle varies depending on the distance behind the gust generator.

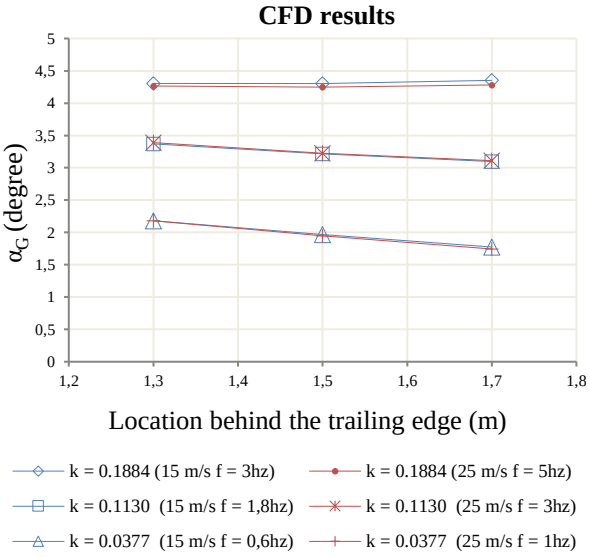

Fig. 8 The maximum gust angle measured at three different locations and reduced frequencies. δ_{max} = ±10 degrees.

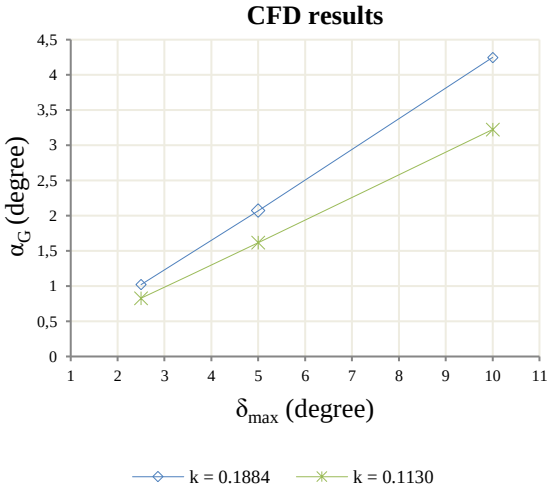

Fig. 9 The maximum gust angle measured for three different δ_{max} and two different reduced frequencies.

Finally the influence of the maximum gust vane deflection is investigated. As can be seen in Fig. 9, there is a linear relation between deflection angle and the maximum gust angle. As also observed by (Brion et al., 2015), a higher reduced frequency results in a larger gust amplitude.

In conclusion, the preliminary CFD study shows that the gust amplitude increases linearly with the vane chord length and the maximum deflection angle. Furthermore, increasing the reduced frequency also induces a stronger gust. Decreasing the space between the gust vanes also increases the gust amplitude, but it leads to a non-uniform gust, which can potentially reduce the quality of the experiment.

2.3 Open Jet Facility

The Open Jet Facility (OJF) at the Delft University of Technology is a low subsonic wind tunnel powered by a 500 kW turbine. The test section, as shown in Fig. 10, has a width and height of 2.85 m. The closed circuit of the OJF, shown in Fig. 11, produces flow speeds up to 35 m/s in a controlled temperature environment.

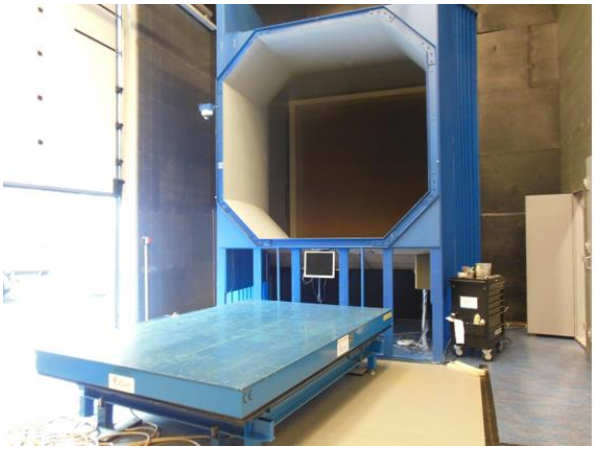

Fig. 10 Interior of the Open Jet Facility at the Delft University of Technology.

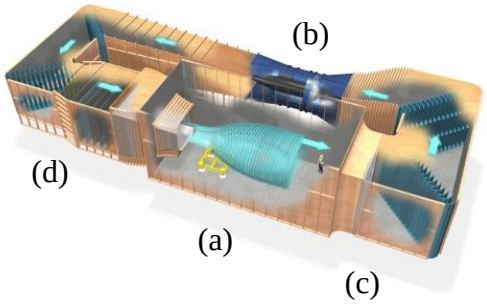

Fig. 11 Schematic of the OJF's closed circuit. (a) is the test chamber, (b) the turbine, (c) the cooling system and (d) the grids and filters to reduce turbulence in the flow.

2.4 Gust generator frame design

As shown in Fig. 12, the frame is made of aluminium rectangular and extruded profiles and designed to be fixed to the ground. The truss members are joined using bolts, T-slot nuts, brackets and specially designed attachment plates.

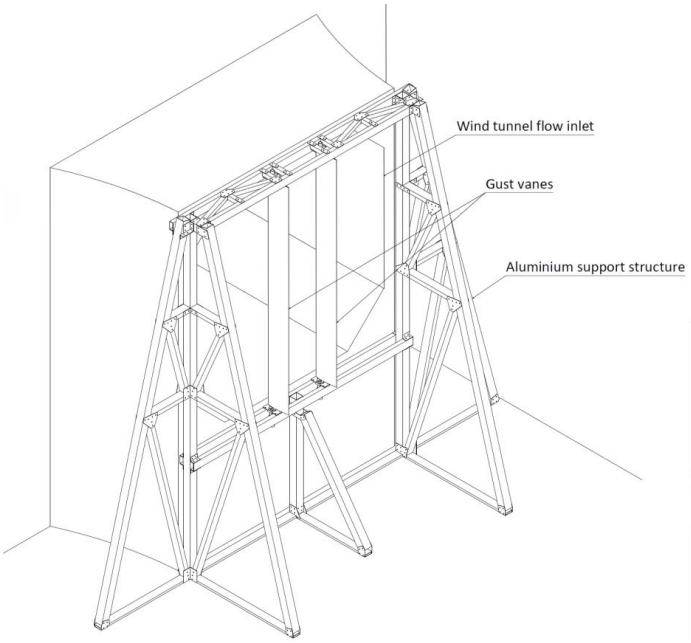

Fig. 12 Sketch of the design of the gust generator and how it is positioned in the Open Jet Facility.

The frame supports the gust vanes and the actuators. In order not to interfere with the airflow, it is built around the flow outlet of the wind tunnel. The gust vanes are currently mounted vertically in the frame, but can also be mounted horizontally if necessary.

One of the design challenges is to ensure that the frame will not resonate within the gust vanes oscillating frequency range. For that purpose, numerous finite element simulations using a beam element model have been done to obtain the present design. With this configuration, the first natural frequency shown in Fig. 13, is 28.4 Hz and is clear from the maximum operational frequency of 5 Hz.

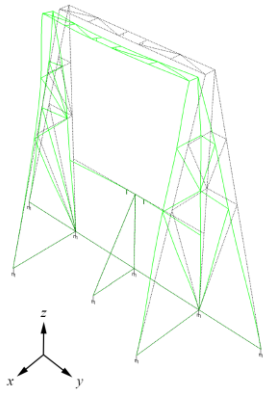

Fig. 13 First mode at 28.4 Hz. The frame is fully attached on the ground.

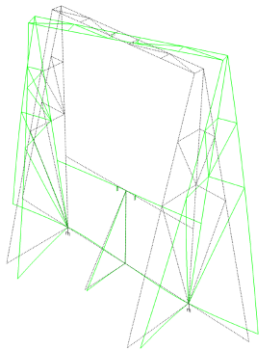

Fig. 14 First mode shape at 3.4 Hz with only two attachment points on the ground.

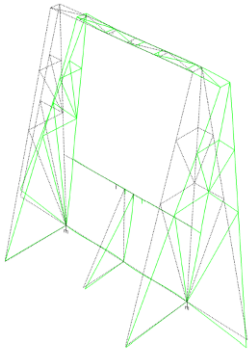

Fig. 15 Second mode shape at 4.5 Hz with only two attachment points on the ground.

However, for the first preliminary experiments with the gust generator, no attachment to the ground was available yet. The natural frequencies of this modified configuration are evaluated with a model having only two attachment points to the ground simulating its weight (200 kg) and providing traction to the ground. As can be observed in Fig. 14 and Fig. 15, the resulting eigen frequencies are significantly lower at 3.4 Hz and 4.5 Hz. The corresponding modes are a torsional mode around the vertical axis and a sideway swaying mode. The torsional mode presents no problem, since induced aerodynamic loads do not excite it considering its shape and the direction in which the aerodynamic loads act (the lift from the gust vanes is along the *y* axis). However, the second mode is excited by the induced aerodynamic loads and, therefore, for the preliminary tests, it has been decided to limit the operational frequency of the gust generator to 4.2 Hz.

2.5 Design of the vanes

The gust vanes are made from Evonik ROHACELL 31IGF foam. This foam allows for a lightweight design and offers good machinability. The surface is impregnated with epoxy resin to increase its toughness and smoothness. During operation, the gust vanes are subjected to inertial and aerodynamic forces. Hence, it is necessary to ensure that they will not bend or twist excessively, since this could detrimentally affect the flow quality. Therefore, the airfoil thickness

(0.042 m with a NACA0014 airfoil) has been selected such that an aluminium spar can fit inside, to provide the required stiffness, as illustrated in Fig. 16 and Fig. 17. The vanes are 2.88 m long, to cover the full height of the wind tunnel, and to avoid having any support structure in the flow. The chord length is 0.3 m to provide the required gust amplitude.

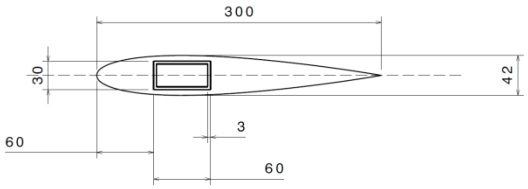

Fig. 16 Dimension of the vane section in mm. The airfoil is a NACA0014.

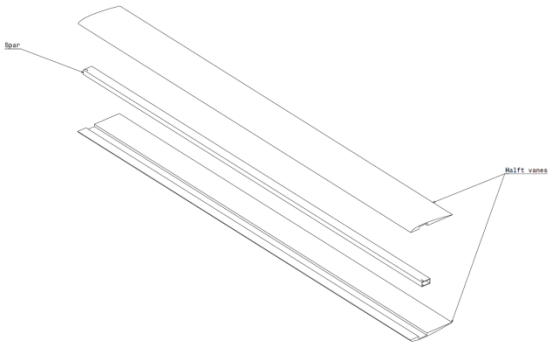

Fig. 17 Two “half vanes” and the aluminium spar.

In order to ensure that the vanes will not experience any resonance vibrations due to their own motion, modal analyses are performed. The vane is fully clamped at one end (simulating the actuator), and is free in torsion on the other end. The first mode, in bending, is at 21 Hz and deemed far enough from the actuation frequency to avoid resonance. Analysis using MSC.NASTRAN showed that the wing is flutter free up to 70 m/s, and that natural frequencies are not affected significantly in the range of flow speeds of the wing tunnel. Additional high fidelity FSI simulations using ANSYS CFX/Structural are done to evaluate the deformation of the gust vanes under unsteady aerodynamic and inertial loads, as illustrated in Fig. 18. The intention was also to evaluate the torque required from the actuators. These simulations are done in 3D, with a structured aerodynamic mesh of 6 million hexahedral elements using similar meshing parameters previously used in the 2D CFD simulations. Walls are located at each ends of the gust vanes to prevent any wingtip vortices and to limit the size of the computational domain. The vane structural model is composed of 6000 non-linear wedge elements discretizing the foam core, and 600 shell elements for the aluminium spar. The simulations are run at a higher flow speed (35 m/s) and gust vane oscillation frequency (10 Hz) than for the experiment, in order to assess robustness of the vane design. The deformations in bending and torsion are monitored at different spanwise locations.

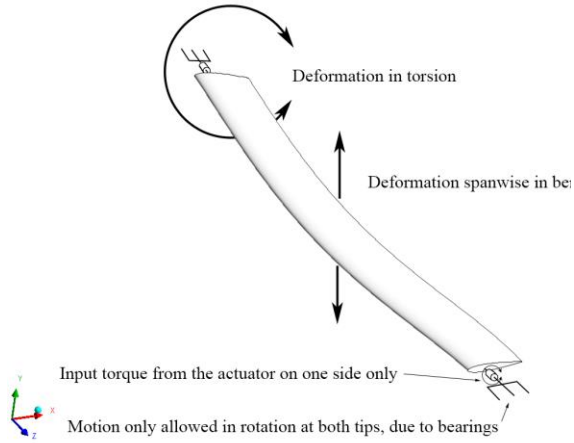

Fig. 18: Schematic illustration of the deformation that a gust vane can experience under inertial and aerodynamic forces.

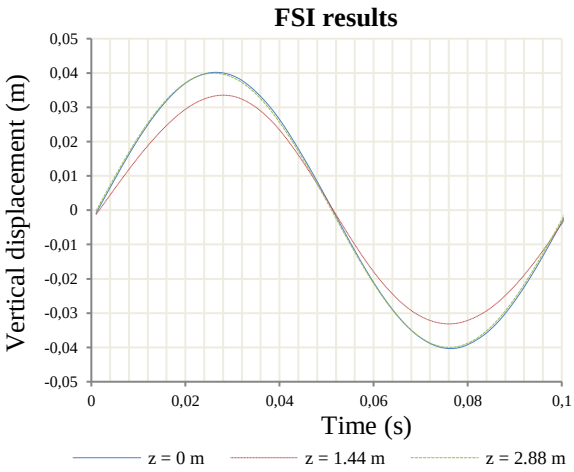

Fig. 19: Computation in time at three locations on the trailing edge of the vanes: at both ends and at mid span.

The vertical displacement of the trailing edge is measured to monitor deformations of the gust vane. The trailing edge is located at a distance of 229 mm from the axis of rotation of the vane and normally experiences a vertical displacement with an amplitude of ± 40 mm when the vane is oscillating without any structural deformation and with $\delta_{max} = \pm 10$ degrees. As can be seen in Fig. 19, the measurement point located at mid span (z = 1.44 m), oscillates with a smaller amplitude (around 33 mm) than both ends of the gust vane, caused by bending of the gust vanes. The negligible differences in deformation between both ends of the gust vane indicates that torsional deformation is negligible and is carried effectively by the aluminium spar.

To measure the impact of the vane deformations on the gust flow, the spanwise variation in gust speed, in the middle between both vanes, is investigated. Fig. 20, shows a side-view of the corresponding wake trailing the gust vanes showing small spanwise gust variations. Fig. 21 shows the gust velocity profiles taken at five different spanwise locations 1.5 m behind the gust generator, showing that the influence of the gust vane deformations on the resulting gust profile is negligible.

Therefore, it can be concluded that the design of the gust vanes is sufficiently stiff and strong, to produce the required gust profiles.

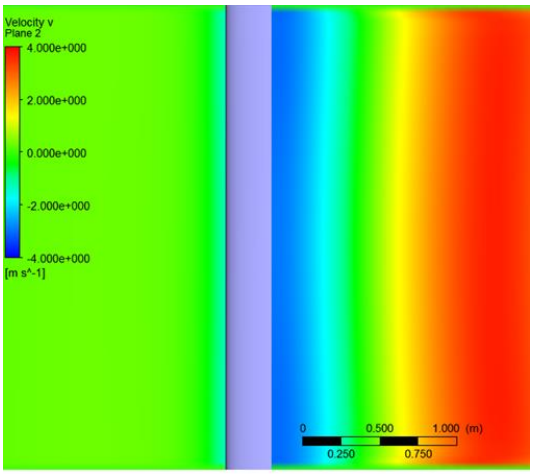

Fig. 20: Contours of the gust velocity in the wake of the vanes for a time transient FSI simulation illustrating the spanwise variation in gust angle.

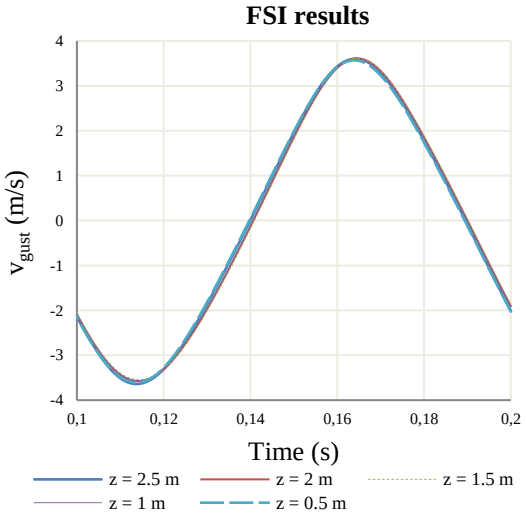

Fig. 21: Velocity profile taken at five different spanwise locations behind the gust generator.

2.6 Actuators and control

Each gust vane was actuated using an actuation system, as shown in Fig. 22, which was purchased from Applied Motion†. The most important properties of the individual components are summarized in the following table:

Table 4 Actuator specifications

Motors			
Operating voltage	48V	Nominal torque	0.56 N.m
Nominal current	5.8 Amps	Rated speed	3350 RPM
Peak current	14 Amps		
Gearheads			
Gear ratio	25:1	Maximum output torque	30.71 N.m
Maximum input speed	5000 RPM		
Servo drives			
Operating voltage	48V	Peak current	14 Amps
Nominal current	7 Amps		
Power supply			
Power	320 Watts	Maximum output current	6.7 Amps

† Applied Motion Products, Inc. 404 Westridge Dr. Watsonville, CA 95076, USA

The actuation system consists of the power supply, regeneration clamp, servo drive, servo motor, and the gearhead. The servomotor is connected to the gust vanes by a gearhead with a 25:1 reduction ratio in order to reduce the power and torque requirements on the servo actuators to oscillate the vanes with the desired frequency and amplitude. The servo drive is programmed to operate in position mode in order to move the servo actuators according to the analog position signal provided by the digital-to-analog converter (DAC) and the gust generator interface, which has been implemented in the National Instruments LabVIEW environment. The servo control unit and the servo motor are connected in a feedback control loop. This way the control unit ensures that the servo motor follows the requested position accurately. Consequently, no feedback control had to be implemented in the gust generator interface, which simplifies the overall control of the gust vane motion.

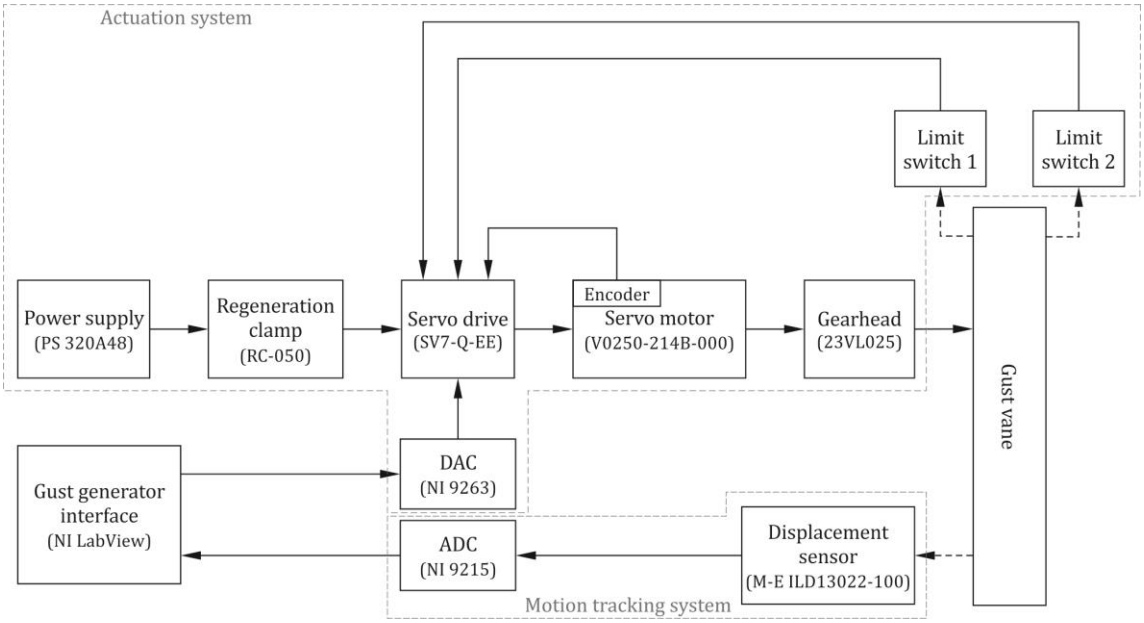

Fig. 22 Gust generator actuation system

However, in order to obtain a smooth motion, the requested position of the gust vane has to be updated with sufficient frequency. Therefore, an analog signal is used as input to the servo drive as a method of communication between the servo drive and the gust generator interface. This way, a position update rate of 1kHz is achieved, meaning that the position of each vane is updated more than 200 times per cycle at the highest tested gust frequency of 4.2 Hz resulting in a smooth motion of the gust vanes over the entire range of operating frequencies .

The actuation system has been augmented with a separate motion tracking system in order to independently track and log the motion of the vanes with respect to the input signal. In this manner

any anomalies in the motion of the gust vanes can be detected and accounted for in any gust response simulations based on the experimental results.

The motion monitoring system consists of a laser displacement sensor mounted at the foot of each vane and an analog-to-digital converter (DAC) to feed the measured signal into the gust generator interface, where the acquired data is processed and logged.

3. Experiment and results

In order to assess the performance of the gust generator, measurements are done for a range of flow speeds, frequencies of actuation, vane deflection amplitudes (± 2.5, ± 5 and ± 10 degrees) and locations (see Table 3 and Fig. 23). Since the frame could not be attached to the ground for the preliminary wind tunnel tests, as discussed in section 2.4, no measurement was carried out at a reduced frequency of 0.1884 and a velocity of 25 m/s, since the corresponding frequency of 5 Hz is beyond the resonance frequency of the frame.

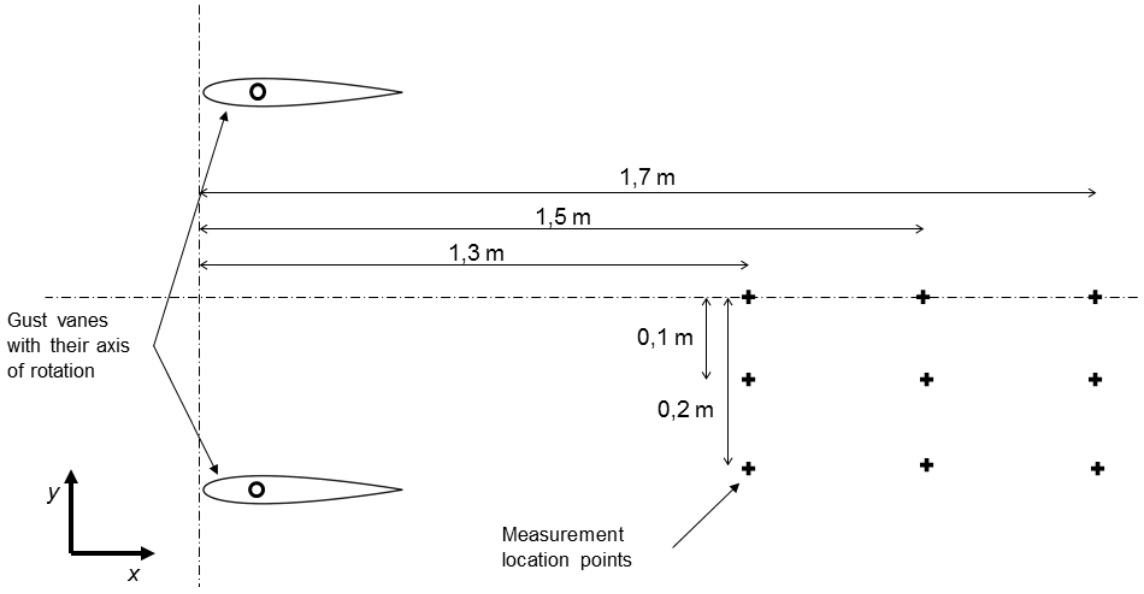

Fig. 23 Schematic of the different positions for the measurements.

3.1 Experimental setup

The system to measure the gust velocity uses a single hot wire anemometer, coupled with a pitot tube as shown in Fig. 24 and Fig. 25. This equipment is mounted on a traversing system, allowing measurements at different locations in space. Measurements are conducted at the center

of the test section at a height of z = 1.5 m, to provide a suitable comparison with the 2D CFD results.

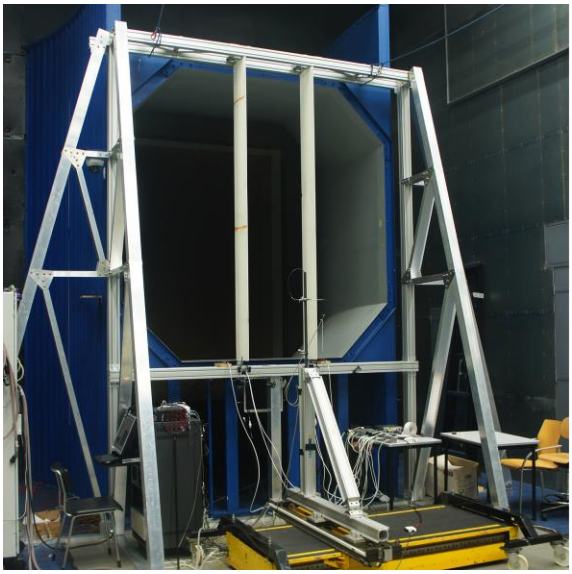

Fig. 24 The gust generator in the wind tunnel. In yellow, the translation system.

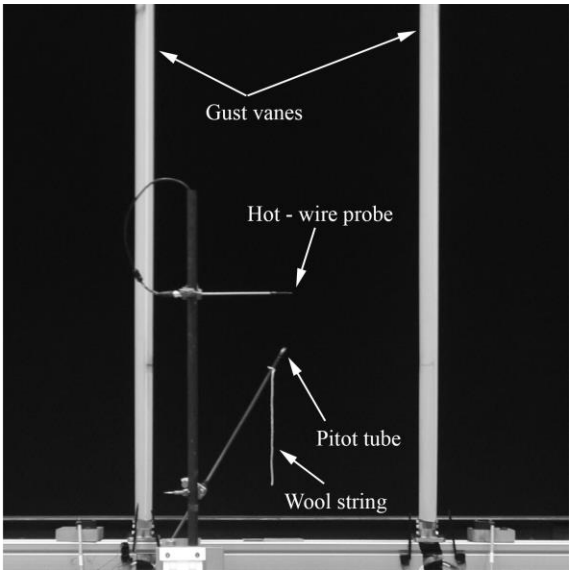

Fig. 25 The different measurement devices

In order to measure the gust velocity a hot-wire anemometer has been used. A hot-wire is mainly sensitive to flow variations normal to the wire. By positioning the wire parallel to the free stream flow, the velocity induced by the gust generator can be measured, as shown in Fig. 26. However, since the gust speed is much smaller than the principal flow speed, the accuracy of the measurements is influenced by small variations in the principal flow speed. As the gust velocity increases, the principal flow velocity slightly decreases, and, therefore, ideally a cross-wire arrangement would be preferred to provide accurate measurements of both components and single out the effect of the gust velocity only. However, because of the availability of measurement equipment, only a single-wire hot-wire was available, and, therefore, the measurements can only be used to evaluate trends, while the exact gust amplitudes are affected too much by measurement uncertainty introduced by the variations in the principal flow component to be able to make any claims in relation to the numerical results.

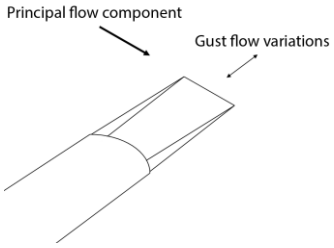

Fig. 26 Schematic of the hot wire probe. The hot wire is used to measure flow variation normal to the wire direction.

3.2 Data processing

The measurements with the hot wire are recorded over 30 seconds, at a sampling frequency of 10 kHz. As shown in Fig. 27, the initial measurements have a low signal to noise ratio and a low pass filter is used to isolate the signal of interest. The low pass cut-off frequency is four times the actual frequency of actuation. As can be seen in the FFT in Fig 28, two frequencies are present in the measured gust signal: (i) at the gust frequency and (ii) at double the gust frequency. First of all, the probe cannot distinguish a positive and negative gust velocity, resulting in a measured signal at double the gust frequency. Second, due to the probe's orientation (horizontal and perpendicular to the free stream flow), the gust flow in one direction is shadowed by the probe, while in the other direction the free gust velocity is measured, resulting in slight differences between the positive and negative gust amplitude, leading to the smaller peak at the gust frequency.

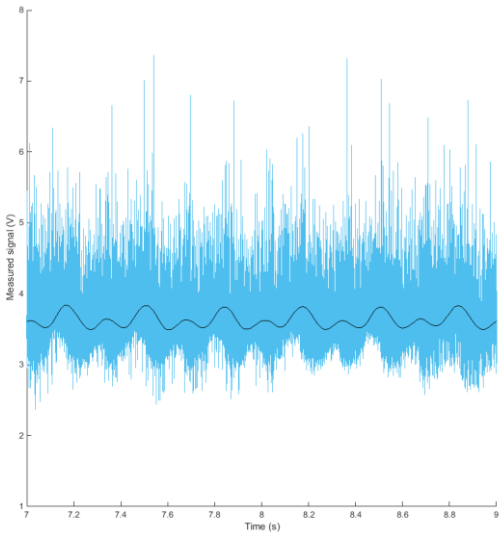

Fig. 27 Raw data and the filtered signal in time.

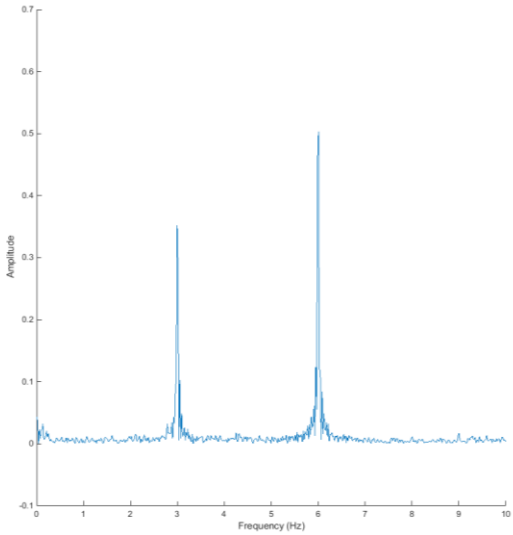

Fig 28 FFT on the raw signal after removing the baseline amplitude. In this example the actuation frequency is 3 Hz.

3.3 Comparison between CFD and experimental results

In this section, the measured gust angle is compared to CFD predictions. Experimental results for the gust angle are shown in Fig. 29. A similar linear dependency between the gust angle and the vane deflection can be observed as in the CFD results shown in Fig. 9. It can also be seen that a higher reduced frequency results in a slight increase in gust amplitude, as also observed in the CFD simulations. Fig. 30 shows a comparison between numerical and experimental results for the gust amplitude. Each dataset is normalised with the gust angle at maximum vane. The results provide a qualitative comparison of the measured trends versus the expected trends, showing good agreement, thus providing some validation of both the numerical results and the gust generator performance.

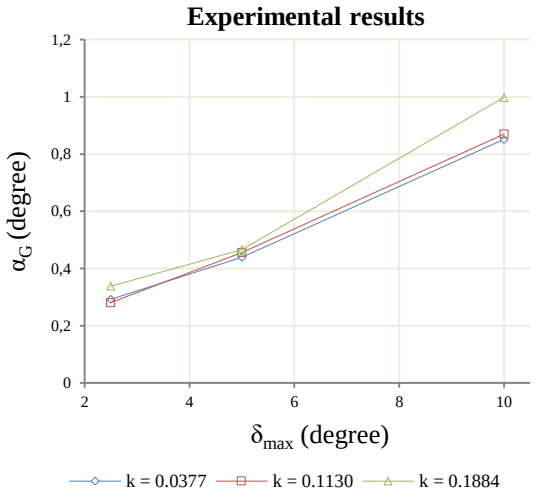

Fig. 29 Maximum gust angle for different vane's deflection and reduced frequency.

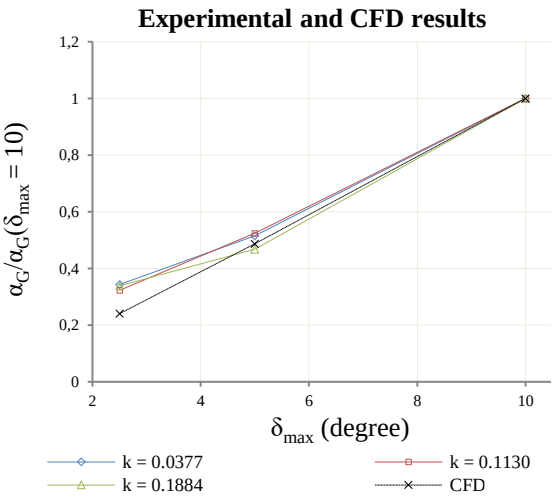

Fig. 30 Normalised maximum gust angle for different vane deflection and reduced frequency.

Measured maximum gust angle as a function of streamwise position is shown in Fig. 31. Depending on the streamwise location behind the gust vanes, a different maximum gust angle is encountered. Comparison of the experimental measurements with the CFD results is shown in Fig. 32, clearly showing that further assessment of the gust generator with more accurate flow measurement techniques (e.g. particle image velocimetry (PIV) or a cross-wire hot-wire anemometer) is required to determine the origin of the discrepancies between the CFD results and the experiments.

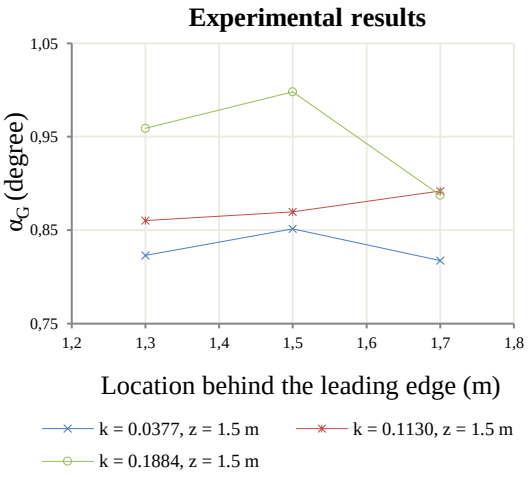

Fig. 31 Maximum gust angle for different locations behind the gust vanes and reduced frequency. δ_{max} = ±10 degrees.

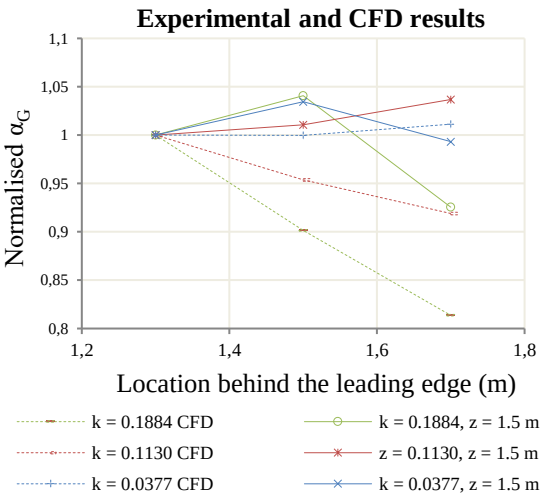

Fig. 32 Same as Fig. 31, but compared with the CFD results. The data are normalised with respect to the values at 1.3 m behind the leading edge for each series.

3.4 Visual observations

In order to investigate the gust angles generated by the gust generator in more detail, a tuft is attached to the pitot tube with which the flow direction and hence the gust angle can be estimated.

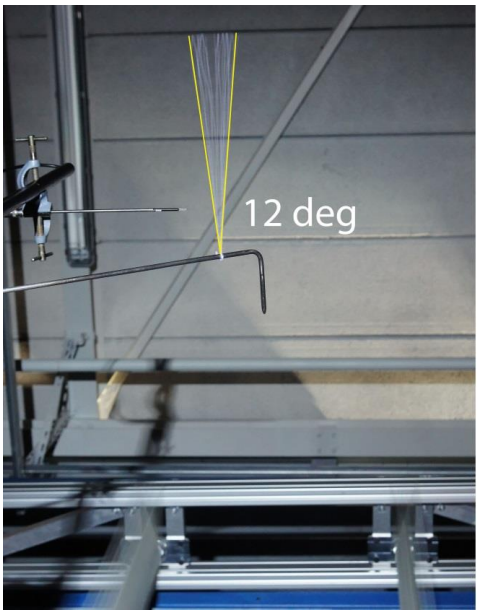

Fig. 33: k = 0.0377 and δ_{max} = ±10 degrees.

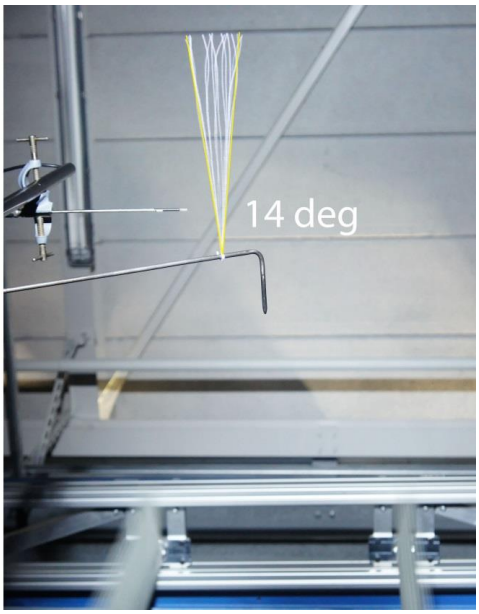

Fig. 34: k = 0.1884 and δ_{max} = ±10 degrees.

Fig. 33 and Fig. 34 show a long exposure shot using stroboscopic light in the dark, to capture the variation of gust angle in time. The camera is located two meters below the string, outside the wind tunnel flow. The cone spanned by the string shows a time history of the flow direction and can be used as an estimate of the full amplitude of the gust (2 times the gust angle). The results show a gust angle of 6 deg for k = 0.0377 and 7 deg for k = 0.1884, showing the dependency of the gust angle on reduced frequency and showing a better than predicted gust generator performance.

Finally, in order to illustrate the development of the gust in flow direction, smoke visualization has been used, as shown in Fig. 35 and Fig. 36.

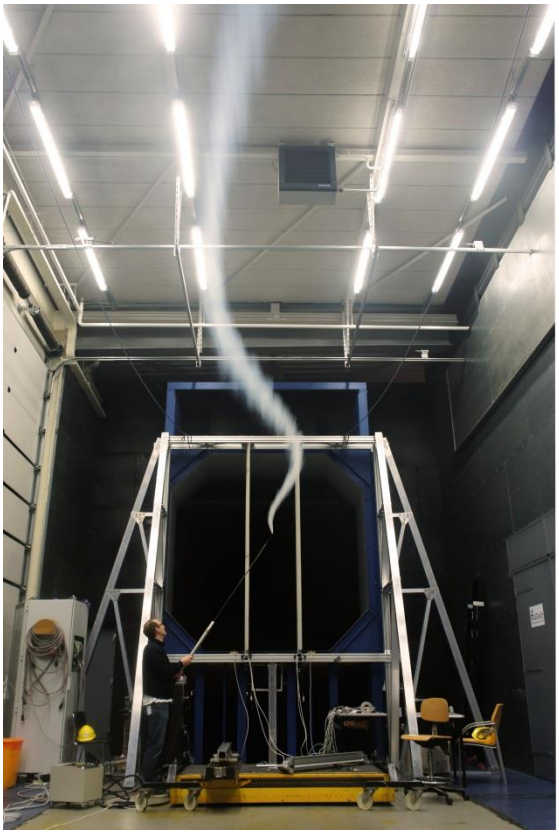

Fig. 35 k = 0.1884 and δ_{max} = ±10 degrees.

Fig. 36 k = 0.3768 and δ_{max} = ±10 degrees.

4. Conclusion

The design and preliminary experimental evaluation of the gust generator constructed at the Delft University of Technology have been presented. The design phase consisted of 2D high fidelity CFD simulations, in order to identify and determine the key design parameters influencing the generated gusts. 3D FSI simulations were performed to assess whether the final design meets the requirements.

Experimental results have been obtained using a single-wire hot-wire anemometer showing a lower gust angle amplitude than predicted by the CFD simulations, and using visual observations revealing stronger gusts than measured by the hot-wire measurements or predicted by the CFD simulations. These discrepancies in the results can probably be explained by the limited accuracy of a single-wire hot-wire measurement setup for assessment of the gust angle and by the fact that CFD simulations are done within a simplified fluid domain. Nonetheless, the relation between the gust angle and the vane deflection shows good agreement between experimental and numerical results. Furthermore, a dependency of the gust on the reduced frequency could clearly be observed.

In conclusion, the first assessment of the performance of the gust generator showed proper operation of the gust generator across the entire range of interest. Additional test campaigns are required to provide a more detailed assessment of the gust generator performance both with and without a test wing present.

5. Acknowledgement

The authors would like to thank Evonik Industries AG for providing the foam for the gust vanes, as well as the technicians from the Delft University of Technology for their help and support in the construction of the gust generator and during the wind tunnel tests. Finally, the authors would like to thank Dr. Terence Macquart from the Delft University of Technology for his help on the control system.

6. References

Allen, N.J., Quinn, M.(2015), "Development of a Transonic Gust Rig for Simulation of Vertical Gusts on Half-models", 31st AIAA Aerodynamic Measurement Technology and Ground Testing Conference. American Institute of Aeronautics and Astronautics, Dallas, TX, USA, June

Brion, V., Lepage, A., Amosse, Y., Soulevant, D., Senecat, P., Abart, J.C., Paillart, P. (2015), "Generation of vertical gusts in a transonic wind tunnel", *Exp. Fluids* **56(**145)

Certification Specifications for Normal, Utility, Aerobatic, and Commuter Category Aeroplanes CS23 Amendment 3 (2012), European Aviation Safety Agency, Köln, Germany

Dequand S., Liauzun C., Girodroux-Lavigne P., Lepage A. (2011), "Transonic response to a gust", International Forum on Aeroelasticity and Structural Dynamics, Paris, France, June

Grissom, D., Devenport, W. (2004), "Development and Testing of a Deterministic Disturbance Generator", 10th AIAA/CEAS Aeroacoustics Conference. American Institute of Aeronautics and Astronautics, Manchester, England, May

Ham, N.D., Bauer, P.H., Lawrence, T.L. (1974), "Wind Tunnel Generation of Sinusoidal Lateral and Longitudinal Gusts by Circulation of Twin Parallel Airfoils", NASA CR 137547, Massachusetts Institute of Technology, Cambridge, MA, USA

Cal Poly Pomona Gust Generation System (2013), https://www.youtube.com/watch?v=FTC0giGEjpk, California Polytechnic University Pomona, Pomona, CA, USA

Koushik, S., Schmitz, F. (2008), "A New Experimental Approach to Study Helicopter Blade-Vortex Interaction Noise", 14th AIAA/CEAS Aeroacoustics Conference (29th AIAA Aeroacoustics Conference), Vancouver, BC, Canada, May

Kuzmina, S., Ishmuratov, F., Zichenkov, M., Chedrik, V. (2005), "Analytical-Experimental Study on Using Different Control Surfaces to Alleviate Dynamic Loads" 47th AIAA/ASME/ASCE/AHS/ASC

Structures, Structural Dynamics, and Materials Conference. American Institute of Aeronautics and Astronautics, Newport, RI, USA, May

Lepage, A., Amosse, Y., Le Bihan, D., Poussot-Vassal, C., Brion, V., Rantet, E. (2015), "A complete experimental investigation of gust load : from Generation to active control", International Forum on Aeroelasticity and Structural Dynamics, Saint Petersburg, Russia, June

Neumann, J., Mai, H. (2013), "Gust response: Simulation of an aeroelastic experiment by a fluid–structure interaction method." *J. Fluids Struct*. **38**, 290–302

Reed, W.H. (1981), "Aeroelasticity matters: Some reflections on two decades of testing in the NASA Langley transonic dynamics tunnel" Intern. Symp. on Aeroelasticity, Nuremberg, Germany.

Ricci, S., Scotti, A. (2008), "Wind Tunnel Testing of an Active Controlled Wing Under Gust Excitation", 49th AIAA/ASME/ASCE/AHS/ASC Structures, Structural Dynamics, and Materials Conference. American Institute of Aeronautics and Astronautics, Schaumburg, IL, USA, April

Roadman, J., Mohseni, K. (2009), "Gust Characterization and Generation for Wind Tunnel Testing of Micro Aerial Vehicles", 47th AIAA Aerospace Sciences Meeting Including The New Horizons Forum and Aerospace Exposition. American Institute of Aeronautics and Astronautics, Orlando, FL, USA, January

Saddington, A.J., Finnis, M.V., Knowles, K. (2015), "The characterisation of a gust generator for aerodynamic testing" *Proc IMechE Part G: J Aerospace Engineering*, **229(**7) 1214-1225

Kenichi, S., Shunsuke, K., Koichi, S. (2015), "Test and analysis of a gust generator for a transonic wind-tunnel." International Forum on Aeroelasticity and Structural Dynamics, Saint Petersburg, Russia, June

Ricci, S., Adden, S., Servadio, C., Karpel, M. and Cooper, J. (2015), "Wind tunnel experimental validation of future green regional a/c gust load alleviation control system.", International Forum on Aeroelasticity and Structural Dynamics, Saint Petersburg, Russia, June

Tang, D.M., Cizmas, P.G.A., Dowell, E.H. (1996), "Experiments and analysis for a gust generator in a wind tunnel.", *J. Aircr*. **33**, 139–148

Test fixture, http://www-en.santech.co.jp/test-research/test-fixture, San Technologies Co., LTD., Shirakuwada, Kanuma-shi, Tochigi-ken 322-0011, Japan

Wu, Z., Chen, L., Yang, C. (2013), "Study on gust alleviation control and wind tunnel test.", *Sci. China Technol. Sci*. **56**, 762–771